Subcascade formation and defect cluster size scaling in high-energy collision events in metals

A. de Backer, A.E. Sand, K. Nordlund, Laurence Luneville, D Simeone, S.L. Dudarev

A Letters Journal Exploring the Frontiers of Physics

July 2016

EPL, **115** (2016) 26001 www.epljournal.org
doi: 10.1209/0295-5075/115/26001

Subcascade formation and defect cluster size scaling in high-energy collision events in metals

A. De Backer[1], A. E. Sand[2], K. Nordlund[2], L. Luneville[3,4], D. Simeone[4,5] and S. L. Dudarev[1]

[1] *CCFE, Culham Science Centre - Abingdon, Oxon OX14 3DB, UK*
[2] *Department of Physics, University of Helsinki - P.O. Box 43, FI-00014 Helsinki, Finland*
[3] *CEA/DEN/DANS/DMN/SERMA/LLPR-LRC CARMEN, CEA Saclay - F-91191 Gif-sur-Yvette, France*
[4] *Centralesupelec/SPMS/LRC CARMEN - F-92292 Chatenay Malabry, France*
[5] *CEA/DEN/DANS/DMN/SRMA/LA2M-LRC CARMEN, CEA Saclay - F-91191 Gif-sur-Yvette, France*

received 15 April 2016; accepted in final form 13 July 2016
published online 17 August 2016

PACS 61.80.Az – Theory and models of radiation effects
PACS 61.82.Bg – Metals and alloys
PACS 61.72.J- – Point defects and defect clusters

Abstract – It has been recently established that the size of the defects created under ion irradiation follows a scaling law (Sand A. E. *et al.*, *EPL*, **103** (2013) 46003; Yi X. *et al.*, *EPL*, **110** (2015) 36001). A critical constraint associated with its application to phenomena occurring over a broad range of irradiation conditions is the limitation on the energy of incident particles. Incident neutrons or ions, with energies exceeding a certain energy threshold, produce a complex hierarchy of collision subcascade events, which impedes the use of the defect cluster size scaling law derived for an individual low-energy cascade. By analyzing the statistics of subcascade sizes and energies, we show that defect clustering above threshold energies can be described by a product of two scaling laws, one for the sizes of subcascades and the other for the sizes of defect clusters formed in subcascades. The statistics of subcascade sizes exhibits a transition at a threshold energy, where the subcascade morphology changes from a single domain below the energy threshold, to several or many sub-domains above the threshold. The number of sub-domains then increases in proportion to the primary knock-on atom energy. The model has been validated against direct molecular-dynamics simulations and applied to W, Fe, Be, Zr and sixteen other metals, enabling the prediction of full statistics of defect cluster sizes with no limitation on the energy of cascade events. We find that populations of defect clusters produced by the fragmented high-energy cascades are dominated by individual Frenkel pairs and relatively small defect clusters, whereas the lower-energy non-fragmented cascades produce a greater proportion of large defect clusters.

Introduction. – Changes in physical and mechanical properties of materials, exposed to neutron and ion irradiation in nuclear reactors, fusion devices, or particle accelerators, result from the generation of defects, their clustering, the formation of dislocation loops and dislocations, and the subsequent evolution of radiation-induced microstructure driven by diffusion and interactions between the defects. In alloys, including those formed due to transmutation nuclear reactions [1], chemical segregation also occurs, resulting in the formation of helium bubbles [2–4], chromium or rhenium precipitates [5,6], and giving rise to grain boundary embrittlement [1,7]. Interpreting the observed microstructural evolution effects requires extending the measure of radiation damage beyond the *displacement per atom* (dpa) concept, proposed by Norgett *et al.* [8] to quantify the exposure of materials to fluxes of energetic particles [9]. Defining a physical measure of accumulation of defects in materials under collision cascade conditions involves recognizing the fact that clusters of defects form directly in collision cascade events [10,11]. Sand *et al.* [12] and Yi *et al.* [13] showed that the statistics of defect cluster sizes formed in relatively low-energy cascades is well described by a power law distribution, similar to the power law describing the statistics of fragmentation of objects [14]. However, there remains an outstanding question that simulations and

observations performed in refs. [12,13] did not address. The question concerns the role played by the fragmentation of cascades themselves. Such fragmentation occurs if the energy of a primary knock-on atom (PKA), initiating a cascade event, exceeds a certain threshold value. What remains unexplored is the effect of cascade fragmentation on the statistics of defect clusters. In this letter we investigate and answer this question.

Cascade fragmentation is a phenomenon occurring if the energy of a PKA produced by an incident neutron or ion [1] exceeds a threshold value, which is close to 30 keV in iron and 160 keV in tungsten. This is a high-energy phenomenon that can be reasonably well described by a treatment that neglects the many-body aspects of interatomic interactions involving valence electrons. Molecular-dynamics (MD) simulations of cascade fragmentation [15] show that the fundamental character of defect clusters formed in high-energy cascade events does not change above the fragmentation threshold. On the other hand, the formation of subcascades may influence the defect cluster size distribution. The statistics of subcascade fragmentation was first investigated by Hou [16], who developed a fuzzy clustering method and applied it to the study of cascades in Au. Satoh *et al.* [17] proposed a model for cascade fragmentation and investigated high-energy cascades in Al, Cu and Au, exploring the dependence of cascade configurations on atomic number and density. Heinisch and Singh [18] performed an extensive study of cascade fragmentation in several fcc, bcc, and hcp metals. Jumel *et al.* [19] used an analytical approach based on the binary collision approximation (BCA), which they applied to predict subcascade spectra in iron produced by neutrons in High Flux Irradiation Reactor of Oak Ridge National Laboratory. Simeone *et al.* and Luneville *et al.* [20,21] extended the work by Cheng *et al.* [22] and developed a fractal approach to the treatment of cascades. Cascade fragmentation correlates primarily with the atomic charge. The threshold energy for cascade fragmentation is identified from the statistics of subcascades and distances between them. A recent example, illustrating the effect of cascade fragmentation on the defect cluster size population, is provided by MD simulations of very high-energy cascades in Fe performed by Zarkadoula *et al.* [23]. Simulations show that populations of defects formed in 500 keV cascades are visibly dominated by individual Frenkel pairs and relatively small defect clusters, with almost no large defect clusters present in the cascade debris. Our analysis, given below, explains this effect and generalizes it to a broad range of materials and irradiation conditions.

We use a binary collision approximation (BCA) model to investigate the spatial repartition of the energy of the projectile that results from the primary recoil and subsequent atomic collisions. Thanks to its relative simplicity, our model can be applied to a pure material or alloy, and to a broad range of incident particles —neutrons or ions— initiating cascade events. Our treatment of cascade fragmentation is focused on the formation of sub-domains. This produces statistical information that can be combined with the data on defect formation dur- ing recrystallization, deduced from MD simulations. Our method is different from earlier simulations by Broeders *et al.* [24] in that we take full cascade information into account and relate the volumes of subcascades to equivalent effective secondary knock-on atom (SKA) energies, in this way mapping the statistics of sub-domain volumes to the global distribution of defect cluster sizes associated with an entire fragmented or non-fragmented cascade event.

The sub-domain decomposition approach combines a BCA treatment of the cascade with a method for the identification of one or several distinct regions of high density of deposited energy. We apply the model to W and Fe and investigate the statistics of cascade events in these two materials, exploring the dependence of sub-domain distributions as a function of their volume and the PKA energy. We analyze the dependence of cascade fragmentation on the atomic number and mass density of the material, and establish a statistical law defining the population of defect cluster sizes produced in an entire cascade event. Our analysis explains the increase of the effective power law exponent observed in recent experiments by Yi *et al.* [13], which explains why the defects produced in fragmented cascades contain greater numbers of individual Frenkel pairs and small defect clusters, whereas the non-fragmented cascades are characterised by larger defect clusters and dislocation loops.

Cascade fragmentation. – The Monte Carlo BCA model for atomic collisions implemented in the SDTrimSP code [25,26] is used for simulating cascade evolution at high impact energies. The slowing-down of atoms is modeled, without giving any consideration to the crystal structure, by a series of random collisions and continuous interaction with electrons. The main input parameters describing a target material are its atomic number and density. The slowing-down of knock-on atoms and development of the cascade itself is simulated assuming that moving atoms do not interact. The kinetic energy transferred to the knock-on atom is calculated by the scattering integral using the Ziegler-Biersack-Littmark potential. In the simulations described below, surface effects are not treated, and the term PKA refers to the initial projectile. The model includes two energy loss channels, the kinetic energy transfer in nuclear collisions and the electron energy losses. A BCA model does not treat melting and recrystallization, and hence on its own it cannot fully describe the cascade debris remaining in the material, or the interaction and recombination of defects. To relate BCA simulations to experimental observations, which show the formation of individual subcascades [27], we use a sub-domain decomposition method, where we describe the result of cascade evolution in terms of one or several spatially separated, hence by definition *non-overlapping*, sub-domains. The spatial repartition of the damage is

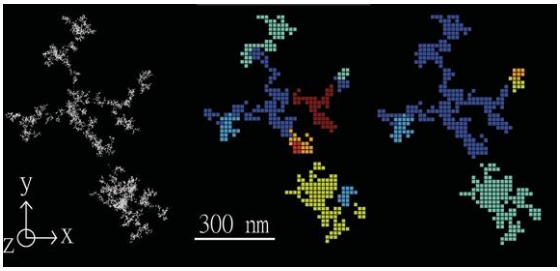

Fig. 1: (Colour online) Left: sketch illustrating a high-energy cascade in tungsten, initiated by a 1 MeV primary knock-on atom, and represented by points where energy was lost in a BCA simulation. Centre: the same cascade represented by a set of elementary cubes (ECs), where the melting criterion (1) was satisfied. The size of ECs used in the simulation was 15 Å. Right: the same cascade, where electronic losses were added to nuclear losses when applying the melting criterion. All the figures are projections onto the (x, y)-plane. The same colour refers to ECs belonging to the same molten sub-domain.

analysed by comparing the amount of energy deposited locally in a certain volume with a local melting criterion, which is derived from certain thermodynamic quantities characterizing the material. A volume large enough to contain the full extent of a cascade is created and divided into elementary cubes (ECs). During the cascade calculation, the energy of the initial projectile is transferred from a knocked-on atom to a knocked-on atom down to the slowest one, the kinetic energy of which is lower than the cutoff energy. An amount of energy equal to the bulk energy is subtracted from the kinetic energy if a vacancy is created, and also the kinetic energy is reduced if electronic losses occur along the free flight paths [25]. These energies are summed in each EC then compared with the amount of energy, E_m, required to melt the material in that particular EC, namely

$$E_m = [C(T_m - T) + L]\,V, \qquad (1)$$

where C and L are the specific heat and enthalpy of fusion, respectively. T_m and T are the melting temperature and the initial temperature of the material and V is the volume of an EC. The above equation cannot describe the melting of the material during the cascade since it is a non-equilibrium process, the specific heat is a function of temperature, and also, given the short timescale, the melting temperature is expected to be around 20% higher than the equilibrium melting temperature [28]. Still this criterion is sufficient to reproduce the liquid volume observed in full MD cascades. Also it provides a suitable numerical input for the model and is fast, simple and compatible with BCA simulations involving many thousand events and many materials. In what follows, an EC where the deposited energy is larger than E_m will be called molten. The evaluation of the melting criterion of a 10 Å size cube of Fe and W gives, respectively, 44 and 77 eV.

After applying the melting criterion to individual ECs, the neighbouring molten ECs are merged by considering

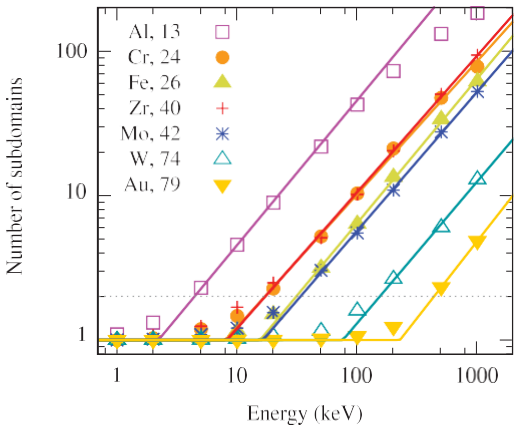

Fig. 2: (Colour online) The number of cascade sub-domains in various metals computed using the domain decomposition method described in the text and plotted as a function of the PKA energy. Lines are fits to simulation data, given by the equation $\nu(E) = 1$ if $E \leq 2^{-1/P} E_{fr}$ and $\nu(E) = 2(E/E_{fr})^P$ if $E \geq 2^{-1/P} E_{fr}$, where ν is the number of sub-domains, E_{fr} is the cascade threshold fragmentation energy, above which cascades start splitting into subcascades, and P varies in the interval from 0.8 to 1.2.

whether any two molten ECs share an edge or a corner. These are then treated as parts of a single molten domain. A full set of connected molten ECs forms a sub-domain. To be treated as separate entities, any two sub-domains must be isolated from each other by a layer of material that does not satisfy the criterion. Such a layer consists of ECs where no collisions occurred, or where the amount of deposited energy is smaller than E_m. Once this procedure has been applied, a cascade can be described as consisting of one or several sub-domains made of individual ECs. The left panel of fig. 1 shows a cascade that formed as a result of impact of an 1 MeV PKA in W. The central panel in fig. 1 shows the same cascade, now analyzed using the domain decomposition procedure, where only nuclear losses were included in the calculation of the deposited energy. The size of the ECs is 15 Å. The right panel in fig. 1 illustrates the same cascade where both nuclear and electron energy losses were included in the deposited energy. The central panel in fig. 1 shows 15 distinct molten sub-domains, whereas we find only 5 separate sub-domains in the right panel. The difference is caused by the narrow connecting molten "tubes" formed due to electron energy losses occurring along the trajectories of fast moving particles. In what follows, we use only the nuclear energy loss criterion to identify the molten sub-domains.

Figure 2 shows the average number of sub-domains generated by PKAs of various energies in different metals. For clarity, only data for seven out of the twenty metals are reproduced here. The full data and comparison with other methods of subcascade fragmentation will be described in [29]. In all the cases we observed a transition from a single molten domain to several sub-domains occurring at a characteristic threshold energy. The total number

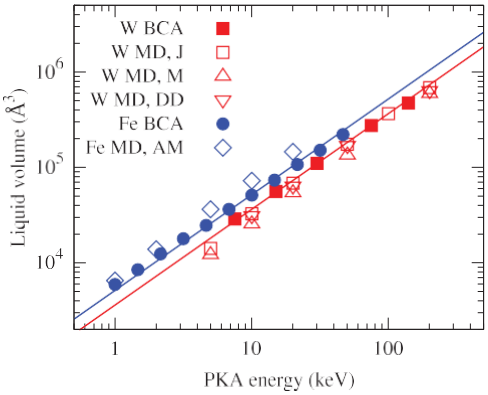

Fig. 3: (Colour online) Comparison of molten volumes of cascades in Fe and W predicted by BCA and MD simulations for various PKA energies. Simulations show that the total volume $V(E)$ of molten material is nearly proportional to the PKA energy. Lines are linear fits of the form $V(E) = V_{fr} \cdot (E/E_{fr})$, where V_{fr} is the volume of the cascade at the fragmentation threshold PKA energy.

of sub-domains v as a function of the PKA energy E is well described by the equation $v(E) = 1$ if $E < 2^{-1/P} E_{fr}$ and $v(E) = 2(E/E_{fr})^P$ if $E \geq 2^{-1/P} E_{fr}$, where E_{fr} is the cascade fragmentation threshold energy, and the fragmentation exponent P varies in the interval from 0.8 to 1.2. The cascade fragmentation transitions occur at PKA energies from 2 keV to 500 keV, which increases with the atomic number and atomic density [29].

To validate eq. (1), we compare the size of *molten volumes* of cascades predicted by MD simulations, with values derived from our BCA-based method. BCA cascade simulations were performed over a broad interval of PKA energies, spanning the range from 1 keV to 10 MeV in W and Fe. It proved necessary to simulate about 1500 cascades per energy to achieve reasonably good statistics. Sub-domain decomposition analysis was then carried out using ECs with sizes varying from 3 to 300 Å. We found a range of values between 10 Å and 20 Å where the results do not depend on the EC size. This justified the choice of EC size used in this study. Averaged molten volumes were compared to MD cascade results over the interval of energies accessible to MD simulations. Figure 3 shows the total volume of cascade molten zones plotted as a function of the PKA energy. The volume of the molten region is proportional to the PKA energy, with cascades in tungsten being more compact than those in iron. The most significant conclusion that we are able to derive from the data shown in fig. 3 is that over a broad range of PKA energies the BCA sub-domain decomposition model predicts the same molten volumes of collision cascades as MD simulations. We now proceed to the analysis of statistics of *sizes* of molten sub-domains produced by PKAs with energies below and above the cascade fragmentation energy. The rationale for performing this analysis is based on the fact that, according to fig. 3, it is possible to establish

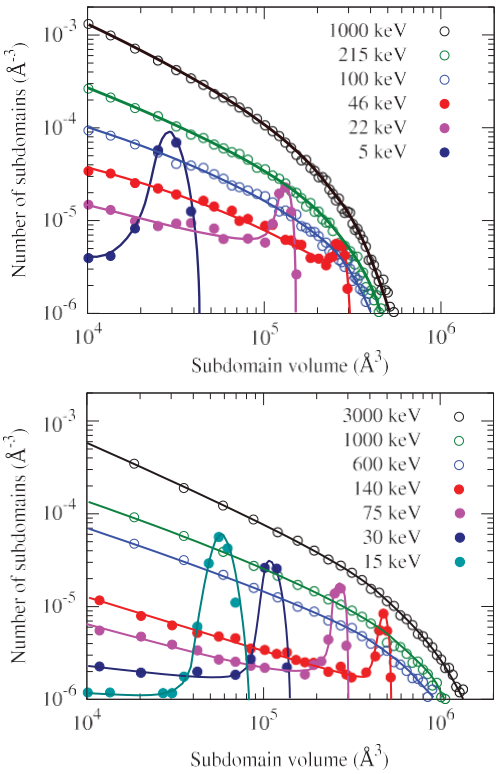

Fig. 4: (Colour online) Distributions of sub-domain volumes in iron (top) and tungsten (bottom) shown as functions of the PKA energy. The distributions are derived from a BCA study involving 1500 cascade simulations performed for every PKA energy.

a unique correspondence between the volume of a molten sub-domain and the energy of an effective secondary knock-on atom (SKA) that produces it. Using this correspondence, and information about the statistics of defect production in individual relatively small cascades [12,13], we will be able to derive a statistical law for defect cluster sizes, describing not only individual relatively low-energy cascades but also high-energy cascades undergoing fragmentation.

Figure 4 shows the average frequency of occurrence of sub-domains plotted as a function of their volume for various PKA energies in tungsten and iron. At PKA energies below the cascade fragmentation transition, the distribution of sub-domain sizes can be approximated by a delta function, which reflects that there is one single sub-domain whose volume is representative of the PKA energy. Around the transition, fluctuations of the volume of the main sub-domain broaden the main peak, which is accompanied by a tail of smaller sub-domains. A fragmented cascade can be viewed as one main sub-domain, due to one SKA whose energy is close to the fragmentation energy, decorated by a one or several sub-domains of smaller effective SKA energy. With PKA energy several times larger than the fragmentation energy, cascades are not characterized by a main sub-domain of a specific size but consist in many sub-domains of any volume whose

occurence decreases with the volume, or equivalently the SKA energy.

We have now established an equivalence between the cascade fragmentation energy threshold, E_{fr}, and a threshold cascade volume, V_{fr}. In principle, this volume is the maximum subcascade or sub-domain volume formed at any energy. However, we have also observed rare sub-domains larger than V_{fr} above the fragmentation transition. They come from the overlap of subcascades from different branches initiated by high-energy knock-on atoms. Since they are rare, we approximate the spectrum of sub-domain volumes shown in fig. 4 by a spectrum of effective SKA energies limited from above by E_{fr}.

In the sub-threshold interval of PKA energies, described by the data shown in fig. 3 for tungsten, it is possible to establish a link between a PKA energy E and a distribution $F(n, E)$ of defect cluster sizes generated by such a PKA [12,13]:

$$E \to F(n, E) = A(E)/n^S, \qquad n < n^*(E), \qquad (2)$$

where for tungsten $S \approx 1.63 < 2$, and $A(E)$ will be defined by a normalization condition on the total number of defects produced in a cascade [8,9]. The upper limit $n^*(E)$ of the number of individual defects in defect cluster is a mere consequence of the finite spatial extent of the cascade. Assuming that defect clusters produced in cascades are dislocation loops with planar geometry, we use the fact that the upper limit on the number of defects in a cluster is proportional to the projected area of a molten zone, which in the sub-threshold energy range $E < E_{fr}$, varies as $n^*(E) \sim E^{2/3}$. This also defined n_{fr}, the size of the largest defect cluster that can be produced in a cascade initiated by a PKA with energy E_{fr}. Because of cascade fragmentation it is also the largest cluster formed in a cascade of *any* energy. With this approach, n_{fr} equals 1450 for a $1/2\langle 111 \rangle$ loop in W, and $n_{fr} = 530$ in Fe.

We now proceed to establish a law of defect clustering also valid above the cascade fragmentation transition. We first consider the distribution $D(\epsilon, E)$ of sub-domains as a function of the SKA energy ϵ. By integrating this distribution $D(\epsilon, E)$ over the energy ϵ of individual sub-domains, we find the total number of sub-domains $\nu(E) = \int_0^E D(\epsilon, E)\mathrm{d}\epsilon$, which is the quantity shown in fig. 2. At energies well below the cascade threshold fragmentation energy the sub-domain energy distribution can be approximated by a single value, $D(\epsilon, E) = \delta(\epsilon - E)$, resulting in $\nu(E) = 1$. At energies close to, or above E_{fr}, the distribution of sub-domain energies is a continuous function of ϵ, spanning the entire interval from zero to E_{fr}. We neglected here the rare subcascade overlap. Now the total number of sub-domains shown in fig. 2 is given by $\nu(E) = \int_0^{E_{fr}} D(\epsilon, E)\mathrm{d}\epsilon$, $E > E_{fr}$. For the PKA energy above the fragmentation threshold energy, the distributions resemble power laws, with a sharp cut-off at the cascade fragmentation energy. The slope of the curves increases slightly as a function of E, showing that at higher energies there appears to be a greater number of smaller sub-domains as opposed to large ones. Fits to the tungsten data using the functional form $D_V(V, E) \propto (V_{fr}/V)^{Q(E)}$ for $V < V_{fr}$ and $E > E_{fr}$ give $Q(E)$ that increases from 0.68 for $E = 300$ keV PKAs to 0.93 for $E = 3000$ keV PKAs. The normalization condition to the total number of sub-domains $\nu(E)$, derived for $Q(E) < 1$, gives that for $E > E_{fr}$ the distribution of sub-domains over energies is

$$D(\epsilon, E) = \nu(E)\frac{1 - Q(E)}{E_{fr}}\left(\frac{E_{fr}}{\epsilon}\right)^{Q(E)}, \qquad (3)$$

where $\epsilon < E_{fr}$.

The distribution of defect cluster sizes for $E > E_{fr}$ can now be evaluated as

$$G(n, E) = \int_0^{E_{fr}} F(n, \epsilon)D(\epsilon, E)\mathrm{d}\epsilon, \qquad (4)$$

where $F(n, \epsilon)$ is given by eq. (2). We need now to define $A(\epsilon)$ for the interval of SKA energy $\epsilon < E_{fr}$. For simplicity, we assume that the total number of individual defects produced in a cascade is a linear function of the SKA energy, as in the Norgett *et al.* model [8]. This results in

$$A(\epsilon) = A_{fr}\left(\frac{\epsilon}{E_{fr}}\right)^{\frac{2S-1}{3}}, \qquad (5)$$

where A_{fr} is a constant. Integrating eq. (4) after replacing $F(n, \epsilon)$ by $A(\epsilon)/n^S$ and $D(E)$ by $\epsilon^{-Q(E)}$ and noting that the lower limit of the integration is defined by the condition that a defect cluster of size n forms only if the energy of a subcascade ϵ exceeds $(n/n_{fr})^{3/2}E_{fr}$, we arrive at

$$G(n, E) \sim n^{-S}\left[1 - \left(\frac{n}{n_{fr}}\right)^{1+S-\frac{3}{2}Q(E)}\right], \quad E > E_{fr}, \qquad (6)$$

where the second term in square brackets describes the effect of cascade fragmentation on the statistics of defect clustering.

The magnitude of the exponent $1 + S - \frac{3}{2}Q(E)$ varies from 1.61 for $E = 300$ keV to 1.23 for $E = 3000$ keV. The factor in square brackets in eq. (6) vanishes when the defect size n approaches n_{fr}. This effect is more pronounced in the limit of high PKA energies.

Figure 5 shows distributions of defect cluster sizes in tungsten, produced by PKAs with energies below and above the cascade fragmentation transition, computed assuming $A_{fr} = 2$. It can be observed that while the maximum size of defect clusters, treated as a function of PKA energy E, increases up to the energy fragmentation threshold, it then remains independent of E. The shape of the defect cluster size distribution as a function of E exhibits a systematic trend, giving greater weight to smaller size defect clusters in cascades produced by higher-energy

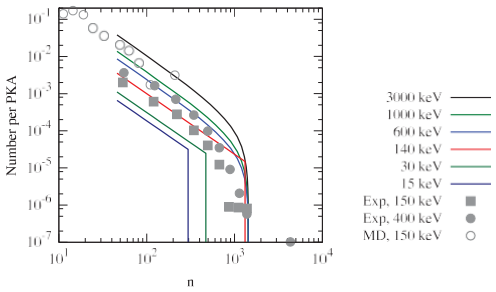

Fig. 5: (Colour online) Distributions of defect cluster sizes in tungsten, produced by PKAs with various energies. Data points are results of MD simulations [12] and experimental electron microscope observations of defect clusters [13]. The slope of the curve at low PKA energies is close to = 1.63. The slope increases to 1.7 for E = 3000 keV.

PKAs. Equation (6) shows that cascade fragmentation limits the formation of large defect clusters, and favors the generation of smaller clusters and individual point defects. This finding, which is a mere consequence of the functional forms of the defect cluster scaling law (2) and the sub-domain energy distribution $D(\epsilon, E)$ shown in fig. 4, appears consistent with MD simulations of very high-energy cascades [23], where defect populations are dominated by individual defects and small defect clusters. It also agrees with the detailed analysis of defect cluster size frequency distributions derived from experimental observations of 400 keV cascades in tungsten [13,30].

While at this point we feel that it would be premature to attempt to identify, at a reasonable level of confidence, the functional form of a global scaling law of defect clustering suitable for all the elements in the periodic table, it appears that the defect cluster size scaling law given by eq. (6) and illustrated in fig. 5 interpolates the data well and may be suitable for practical calculations.

* * *

This work was partly funded by the RCUK Energy Programme (grant No. EP/I501045). The work has been carried out within the framework of the EUROfusion Consortium and has received funding from the Euratom research and training programme 2014–2018 under grant agreement No. 633053. The views and opinions expressed herein do not necessarily reflect those of the European Commission. The work was also supported by CEA/DEN under RSTB/MATIX research program, and by the Enabling Research project TriCEM on Tritium Retention in Controlled and Evolving Microstructure. ADB wishes to thank C. S. Becquart and C. Domain for the many illuminating discussions and encouragements, D. R. Mason for helpful comments on the manuscript, and M. Persson and Kemal Dhennin for their inspiring views.

REFERENCES

[1] Gilbert M. R., Dudarev S. L., Zheng S. *et al.*, *Nucl. Fusion*, **52** (2012) 083019; Gilbert M. R., Marian J. and Sublet J.-Ch., *J. Nucl. Mater.*, **467** (2015) 121.
[2] Becquart C. S. and Domain C., *Phys. Rev. Lett.*, **97** (2006) 196402.
[3] Boisse J., Domain C. and Becquart C. S., *J. Nucl. Mater.*, **455** (2014) 10.
[4] Sandoval L., Perez D., Uberuaga B. P. and Voter A. F., *Phys. Rev. Lett.*, **114** (2015) 105502.
[5] Hardie C. D., Williams C. A., Xu S. and Roberts S. G., *J. Nucl. Mater.*, **439** (2013) 33.
[6] Xu A., Beck C., Armstrong D. E. J. *et al.*, *Acta Mater.*, **87** (2015) 121.
[7] Zhang L., Fu C.-C. and Lu G.-H., *J. Nucl. Mater.*, **459** (2015) 247.
[8] Norgett M. J., Robinson M. T. and Torrens I. M., *Nucl. Eng. Des.*, **33** (1975) 50.
[9] Stoller R., in *Comprehensive Nuclear Materials*, edited by Konings R. J. M. (Elsevier, Amsterdam) 2012.
[10] Diaz de la Rubia T. and Guinan M. W., *Phys. Rev. Lett.*, **66** (1991) 2766.
[11] Woo C. H. and Singh B. N., *Philos. Mag. A*, **65** (1992) 889.
[12] Sand A. E., Dudarev S. L. and Nordlund K., *EPL*, **103** (2013) 46003.
[13] Yi X., Sand A. E., Mason D. R. *et al.*, *EPL*, **110** (2015) 36001.
[14] Oddershede L., Dimon P. and Bohr J., *Phys. Rev. Lett.*, **71** (1993) 3107.
[15] Stoller R., *J. Nucl. Mater.*, **271-272** (1999) 57.
[16] Hou M., *Phys. Rev. A*, **39** (1989) 2817.
[17] Satoh Y., Kojima S., Yoshiie T. and Kiritani M., *J. Nucl. Mater.*, **179** (1991) 901.
[18] Heinisch H. L. and Singh B. N., *Philos. Mag. A*, **67** (1993) 407.
[19] Jumel S. and Van-Duysen J. C., *J. Nucl. Mater.*, **328** (2004) 151.
[20] Simeone D., Luneville L. and Serrys Y., *Phys. Rev. E*, **82** (2010) 011122.
[21] Luneville L., Simeone D. and Weber W. J., *J. Nucl. Mater.*, **415** (2011) 55.
[22] Cheng Y. T., Nicolet M. A. and Johnson W. L., *Phys. Rev. Lett.*, **58** (1987) 2083.
[23] Zarkadoula E., Daraszewicz S. L., Duffy D. M. *et al.*, *J. Phys.: Condens. Matter*, **25** (2013) 125402.
[24] Broeders C. H. M. and Konobeyev A. Y., *J. Nucl. Mater.*, **336** (2005) 201.
[25] Eckstein W., in *Computer Simulation of Ion-Solid Interactions* (Springer, Berlin) 1991.
[26] Mutzke A., Schneider R., Eckstein W. and Dohmen R., SDTrimSP version 5.00, in IPP Report 12/08, MPI für Plasmaphysik (2011).
[27] Jenkins M. L. and Kirk M. A., *Characterization of Radiation Damage by Transmission Electron Microscopy* (IOP Publishing Ltd., Bristol) 2001, pp. 145–158.
[28] Forsblom M. and Grimvall G., *Phys. Rev. B*, **72** (2005) 054107.
[29] De Backer A. *et al.*, in preparation.
[30] Mason D. R. and Yi X., unpublished (2015).